The role of electron current in high-β plasma equilibria ⊕ ⊘

V. A. Kurshakov ; I. V. Timofeev ✉
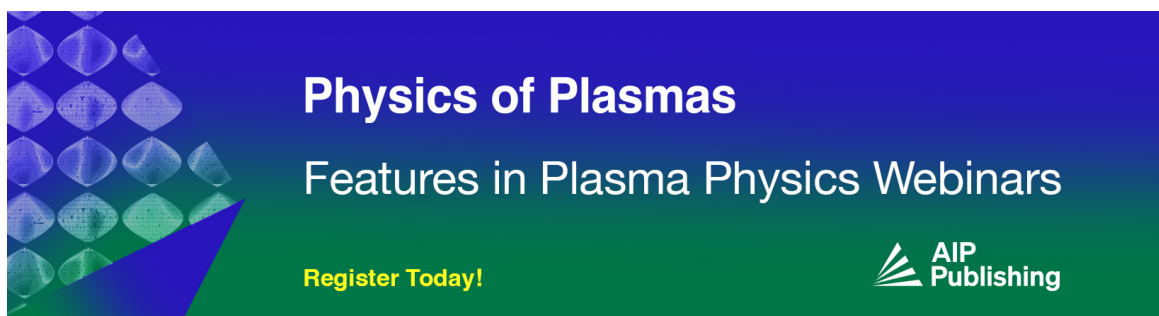
Check for updates

View Online

Export Citation

CrossMark

The role of electron current in high-β plasma equilibria (EP)

View Online   Export Citation   CrossMark

V. A. **Kurshakov**[1,2] (iD) and I. V. **Timofeev**[1,2,a] (iD)

AFFILIATIONS

[1]Novosibirsk State University, Novosibirsk 630090, Russia
[2]Budker Institute of Nuclear Physics SB RAS, Novosibirsk 630090, Russia

[a]Author to whom correspondence should be addressed: timofeev@ngs.ru

ABSTRACT

This paper is aimed at investigating the role of electrons in creation of currents in plasma equilibria with high plasma pressure ($\beta \approx 1$). Despite the long history of studies of these equilibria, there is still no consensus on what kind of particle species is responsible for the creation of the diamagnetic current and what characteristic size the current layer should have. For example, simulations of isothermal plasma injection into a multi-cusp magnetic trap [J. Park *et al.*, Front. Astron. Space Sci. **6**, 74 (2019)] demonstrate the formation of a transition layer with a thickness comparable to the electron Larmor radius, where the equilibrium current is carried by electrons. At the same time, studies of a diamagnetic bubble created by a hot-ion plasma in a mirror trap [I. Kotelnikov, Plasma Phys. Control Fusion **62**, 075002 (2020)] assume ion dominance and completely ignore electron currents. In this paper, we show that the equilibrium initially governed by the ion diamagnetic current is unstable against perturbations at the ion-cyclotron frequency harmonics, and this instability forces the plasma to come to a new equilibrium state in which the current is mainly created by the $\mathbf{E} \times \mathbf{B}$-drift of electrons. The same type of equilibrium is also found to form in a more realistic problem setup when plasma is continuously injected into the uniform vacuum magnetic field.

Published under an exclusive license by AIP Publishing. https://doi.org/10.1063/5.0153855

I. INTRODUCTION

Equilibrium plasma configurations in which the gas-kinetic pressure of the confined plasma P reaches the pressure of the magnetic field $B^2/8\pi$ ($\beta = 8\pi P/B^2 \approx 1$) have been actively studied for more than half a century. The problem of finding an equilibrium boundary between an unmagnetized plasma and an external magnetic field was first considered in relation to the solar wind flow around the Earth's magnetosphere.[1,2] The incoming plasma flow in this case expels the geomagnetic field from its volume and leads to the formation of a relatively narrow transition layer (magnetopause) wherein a jump in the magnetic field strength is produced by a diamagnetic current. At different historical stages of these studies, various alternative models were proposed, in which the role of the main current carrier was assigned to either electrons or ions and the predicted size of the transition layer varied from the hybrid gyroradius $\sqrt{\rho_e \rho_i}$ to the Larmor radius of ions ρ_i.[3,4] The former regime was characterized by the appearance of an electrostatic potential in the transition layer, which is associated with different penetration depths of ions and electrons in the strong magnetic field. Ions cannot perform Larmor rotation in such a narrow layer, being reflected from it by the electric field. In the absence of ion drift motion, the required current is generated mainly by the $\mathbf{E} \times \mathbf{B}$-drift of electrons. In the latter regime, it was assumed that the electric field arising due to charge separation is short-circuited in other regions of the magnetosphere. As a consequence, the diamagnetic current and the layer width are mostly determined by the ion gyration.

Similar studies on the structure of the plasma boundary layer at high pressure $\beta \approx 1$ were also carried out with regard to the laboratory experiments on magnetic fusion devices including θ-pinches[5–7] and cusp magnetic field configurations.[8,9] The first kinetic theories for the simplified problem of the flat boundary equilibrium, both neglecting the electric potential[10] and taking it into account,[11] showed that the transition layer size can be arbitrary and depends on how this layer is "loaded" with trapped particles. In reality, the equilibrium is always dynamic and should depend not only on how the population of trapped particles is replenished, but also how it is depleted. However, it is also obvious that the large pressure gradients formed at the plasma boundary may excite instabilities. Inside an unstable transition layer, the particles transport should be determined by the complicated turbulent processes instead of the classical collisions. Early theoretical and particle-in-cell (PIC) simulations confirmed the development of drift microinstabilities in rather thin transition layers ($\lambda < \rho_i$) in high-β plasma.

For the first time, an instability at harmonics of the ion-cyclotron frequency in a plasma with a density gradient transverse to the magnetic field was discussed in the theoretical paper.[12] It was shown that the instability develops because of the intersection between the ion drift branch and ion-cyclotron oscillations. The applicability of this theory, however, was limited by the low plasma pressure ($\beta \ll 1$) and the absence of an equilibrium electric field. For $\beta \sim 1$, a similar instability was observed in PIC simulations of the solar wind impingement on the Earth's magnetic field.[13] It was shown that the development of instability leads to broadening of the transition layer up to the ion Larmor radius ρ_i. High-β equilibria with an electric field transverse to the plasma boundary and a dominant electron current were actively studied earlier in relation to experiments on θ-pinches.[14] Theoretical predictions about the possibility of developing a lower hybrid drift instability at such a boundary[15–17] were confirmed by pioneering PIC simulations.[18]

At present, interest in the formation of high-β plasma equilibria continues to be supported both by studies of the magnetic holes in space plasmas[19] and by the development of alternative directions of the controlled nuclear fusion among which it is worth mentioning field reversed configurations (FRC),[20–22] as well as multi-cusp[23,24] and mirror traps.[25–29] Recent PIC simulations[30] of equilibrium establishment in a multi-cusp "picket fence" system have shown the importance of a kinetic description of the electron dynamics in the $\beta \approx 1$ regime and demonstrated the possibility of forming a transition layer with a purely electron current and a size comparable to the electron gyroradius ρ_e. In the present paper, we will show that the stability of such a thin current layer observed in these PIC simulations may be the result of the axial symmetry of the problem, which prohibits the existence of any perturbations traveling along the azimuthal drift of particles. An earlier work[30] demonstrates that the small layer width ($\lambda \sim \rho_e$) should lead to a decrease in particle losses from the trap. This conclusion, however, ceases to be obvious if drift instabilities at the ion-cyclotron and lower-hybrid frequencies are developed in the layer, mixing the plasma on the ion Larmor radius scale.

The $\beta \approx 1$ regime is also considered as the most promising one for the concept of a fusion reactor based on a mirror trap. Beklemishev[25] has shown that the equations of MHD equilibrium admit the existence of solutions similar to FRC, where a "diamagnetic bubble" without a magnetic field is formed instead of a region with a reversed field. The width of the transition layer λ in this bubble is estimated from the equality between the time needed for the magnetic field to diffuse through this layer and the typical time of longitudinal gasdynamic losses through mirrors τ_{GD},

$$\lambda = \sqrt{\frac{c^2 \tau_{GD}}{8\pi\sigma}}, \tag{1}$$

where σ is the classical plasma conductivity and c is the speed of light. For the future reactor parameters, the width of this layer turns out to be smaller than the ion Larmor radius, which makes the hydrodynamic approach inapplicable for the description of such an equilibrium. Moving along the path of constructing the kinetic theory of the diamagnetic bubble, Kotelnikov[31] has considered the problem of the collisionless plasma equilibrium with a flat boundary, previously solved by Grad,[10] and generalized it to the case of an axially symmetric plasma column. In Kotelnikov's theory, the typical size of the transition layer has been found to be several gyroradii of ions

($\lambda = (6 - 8)\rho_i$). Also, an important assumption has been made about the possibility of neglecting the electric field arising due to charge separation, which allows one to consider only the currents associated with ion drifts. However, while Grad has limited the applicability of his theory to the electron-positron plasma case ($m_i = m_e$), Kotelnikov has justified this assumption for a hydrogen plasma by the low electron temperature. This assumption, however, contradicts the results of hybrid simulations of the field reversed θ–pinch discharge[32] where electrons were treated as a cold massless fluid and the Hall-driven electric field was found to play a significant role in creation of equilibrium current. The only reason to neglect the electric field may be the short circuit of currents on various magnetic field lines at the ideally conductive end, but the question of how efficiently the electric contact between different lines can be implemented in the presence of strong magnetic mirrors has not yet been answered.

The diamagnetic bubble regime is planned to be implemented in the GDMT project (Gas Dynamic Multiple Mirror Trap),[33,34] in which an equilibrium plasma configuration with a completely expelled magnetic field is supposed to be created using powerful neutral injection. To check the fundamental possibility of achieving such an equilibrium in this way, the CAT experiment (Compact Axisymmetric Toroid)[35,36] is started at the Budker Institute of Nuclear Physics. In this experiment, the injection of neutral beams with a total power of several megawatts should lead to a significant increase in plasma pressure inside a compact mirror cell. Due to the higher density of the injected ion current in the CAT experiment, it is planned to exceed the value of the weakening of the vacuum magnetic field (90%) which was achieved at the 2XIIB facility.[37]

Recent attempts to construct a theory for the stationary equilibrium in the bubble regime are based on a hybrid approach: warm plasma is described in it using resistive MHD with classical transport coefficients in the transition layer,[27] and for a population of fast ions, arising in a trap due to neutral injection and playing the dominant role in creating the diamagnetic current, a simplified kinetic model is used. This theory predicts the possibility of a significant increase in the plasma lifetime in a trap compared to the time of gasdynamic outflow.[33] It is assumed that, experiencing collisional deceleration on electrons without angular scattering, fast ions can accumulate for a sufficiently long time (practically without losses) in the region of absolute confinement.[31,38] Obviously, the losses of particles due to their angular scattering can increase significantly if the diamagnetic current layer is unstable against drift oscillations falling in resonance with the ion-cyclotron harmonics $n\Omega_i$ or lower hybrid waves at Ω_{LH}. In this situation, the time of ion scattering in the trap can be reduced to the time of flight of the diamagnetic bubble diameter, which may lead to the gasdynamic losses of fast ions through the mirrors.

In this work, using PIC simulation, we will show that the $\beta = 1$ equilibrium with even a wide current layer obtained in Ref. 31 is unstable against perturbations at the ion-cyclotron frequency harmonics. When this instability saturates, regardless of the electron temperature, the plasma comes to another equilibrium state in which the ion pressure is held by the electrostatic potential, and the current needed for equilibrium is created by the $\mathbf{E} \times \mathbf{B}$-drift of electrons rather than by diamagnetic drift of ions. In contrast to previous works, where the dominance of electron dynamics has been explained by the formation of a narrow transition layer (ρ_e or $\sqrt{\rho_e \rho_i}$), equilibrium with an electron current observed in our simulations is formed in a wide layer

occupying several gyroradii of ions. We will also show that this insta-bility disappears and the ion current equilibrium remains unchanged if a plasma in 2D simulations is assumed uniform along the drift direc-tion. To confirm that the same instabilities are developed in a more realistic way of creating plasma equilibrium with $\beta \approx 1$, which is implemented in mirror traps using continuous injection of neutrals into a cold target plasma, we also consider the problem when the plasma pressure gradually increases to the limit of $\beta = 1$. Since cold plasma does not create pressure, and its role is reduced only to the ion-ization of fast atoms in the space it occupies, the problem of interest to us can be reduced to the injection of ion-electron pairs into a selected region of vacuum with an initially uniform magnetic field. For the con-venience of comparison with the flat Kotelnikov equilibrium,[31] we will consider the problem of plasma injection in slab geometry. In relation to the forthcoming experiments at the CAT facility, of particular inter-est is the dynamics of the magnetic field exclusion from the injection region and the effect that the conservation of the magnetic moment of particles μ has on this process. Indeed, despite the presence of large magnetic field gradients at the edges of the magnetic well, its deepen-ing with time is found to be well described by a theory that assumes $\mu = $ const.

II. PIC MODEL

To study the stability of 1D plasma equilibrium with $\beta = 1$ and current that is created exclusively by ions,[31] we will use our own 2D3V PIC code which implements the standard explicit Boris[39] and Yee[40] schemes for solving equations of motion and Maxwell's equations. To accurately fulfill the Gauss law, the electric current density in this model is calculated using the Density Decomposition Method of Esirkepov.[41]

In this paper, we consider two formulations of the problem. In the first one, the vacuum magnetic field is directed transversely to the simulation plane [Fig. 1(a)], and in the second one, this field lies in the plane [Fig. 1(b)]. In other words, we assume that the system is homo-geneous either in the magnetic field direction (case 1) or in the dia-magnetic drift direction (case 2).

In the computational domain, we set initial self-consistent distri-butions of particles $f_{i,e}(x, \mathbf{v})$ and magnetic field $\mathbf{B}_0 = (0, 0, B(x))$ that are inhomogeneous in the x coordinate. To the left of the transition layer, the magnetic field vanishes, and the particle distribution becomes Maxwellian. At the left end of the simulation box, we realize the same open boundary conditions as in Ref. 42, i.e., we create a spe-cial buffer which reproduces the same velocity distribution that is observed in first two cells of the computational domain. It allows to reach a plasma continuity at this boundary. Particles from this buffer freely enter the plasma, but plasma particles entering the buffer are deleted. To the right of the transition layer there is a vacuum region with a uniform magnetic field B_v. Periodic boundary conditions for particles and fields are used on the y-boundaries of the domain. In the x-direction, we use absorbing boundary layers inside which all field perturbations are multiplied by the reduction factor and decay to zero. Electrons are initially located in the same places as ions, therefore $\mathbf{E}(0, \mathbf{r}) = 0$ and $\mathbf{B}(0, \mathbf{r}) = \mathbf{B}_0$. In both cases, simulations are carried out with a time step $\Delta t = 0.01 \, \omega_{pe}^{-1}$ and grid steps $\Delta x = \Delta y = 0.02 \, c/\omega_{pe}$, where $\omega_{pe} = \sqrt{4\pi e^2 n_0/m_e}$ is the plasma frequency cal-culated from the maximum plasma density n_0 in the uniform part of the plasma, and e and m_e are the charge and mass of an electron. The
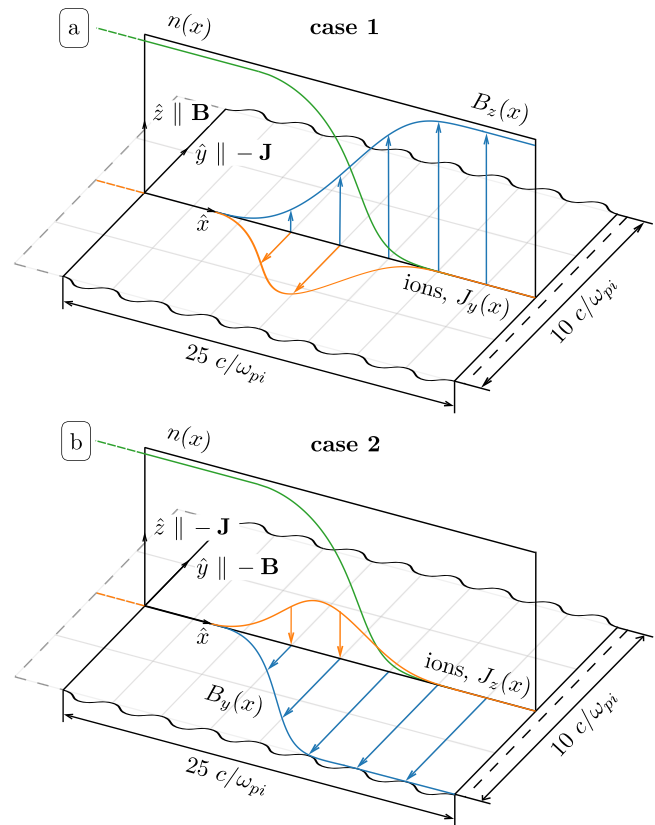
FIG. 1. Layouts of the computational domain for the flat nonuniform kinetic equilib-rium of Kotelnikov with different orientation of magnetic field: (a) $\mathbf{B}_0$ is perpendicular to the simulation plane (x, y) (case 1) and (b) $\mathbf{B}_0$ lies in the simulation plane (x, y) (case 2).

acceptable level of noise is achieved by using 16 macroparticles with the parabolic form-factor in each cell. To reproduce the nonuniform density profile of the plasma with the same level of noise, we keep the same number of macroparticles in a cell at different x, but vary their charges and masses.

Since our goal is to investigate the stability of the equilibrium configuration predicted by Kotelnikov,[31] we chose the regime when electron thermal effects can be completely neglected. It means that not only the pressure of electrons should be a small fraction of ion pressure ($T_e/T_i \ll 1$), but also their thermal velocity should be small compared to the ion thermal velocity ($T_e/T_i \ll m_e/m_i$). In PIC simulations, however, we cannot use an arbitrary small electron temperature. Due to explicit nature of our PIC algorithms, the grid step should be equal to the Debye length. For the step we use in these simulations, the elec-tron temperature is limited by the value $T_e = 200 \, \text{eV}$. The typical tem-perature of ions in mirror traps is determined by the energy of neutral injection and equals to $T_i = 10 \, \text{keV}$. To save calculation time, we use a reduced mass ratio m_i/m_e compared to conventional hydrogen plasma. For $m_i/m_e = 16$, the required condition $T_e/T_i \ll m_e/m_i$ is still satisfied.

To simulate the gradual formation of a high-β plasma equilib-rium, we use the same 2D3V PIC code. In contrast to the evolution of
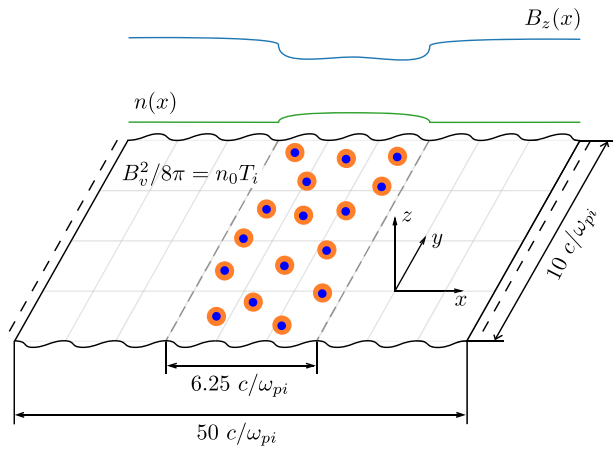
FIG. 2. Layout of the computational domain in the problem of continuous plasma injection.

an equilibrium from a given initial state, here we study the formation of dynamic equilibrium under the continuous injection of plasma into a selected region of space with an initially uniform magnetic field $\mathbf{B_v} \| z$. The layout of the simulation domain with the injection region occupying its central part is presented in Fig. 2. During each time step, a constant number of electron–ion pairs with temperatures $T_i = 10$, $T_e = 2$ keV and the mass ratio $m_i/m_e = 16$ is thrown into this region with a uniform probability in coordinates and with the Maxwellian distribution in velocities so that, by the time τ, the plasma density should grow up to n_0 and the injected ion pressure $n_0 T_i$ should reach the pressure of the external magnetic field $B_v^2/8\pi$. If we take the value $n_0 = 10^{13}$ cm^{-3} as a density unit, the dimensionless vacuum magnetic field $B_v = \sqrt{2T_i/(m_e c^2)} \approx 0.2$ corresponds to the typical magnetic field of the CAT facility (≈ 0.2 T). The injection rate is chosen to be sufficiently small so that during the characteristic time of density increase $\tau = 10^3 \, \omega_{pe}^{-1}$ the ions have time to make two revolutions along the Larmor circle $\tau \approx 4\pi/\Omega_i$ and we do not excite a shock Alfvén wave.

In contrast to the simulations of the Kotelnikov equilibrium, we simulate the regime $T_e/T_i > m_e/m_i$ that is more appropriate for laboratory experiments. Simulations are carried out with the following temporal and spatial resolutions: $\Delta t = 0.025 \, \omega_{pe}^{-1}$ and $\Delta x = \Delta y = 0.05 \, c/\omega_{pe}$. We use absorbing boundary conditions for both fields and particles in the x-direction and periodic conditions along y. The unit density corresponds to 50 computational particles with the parabolic form-factor per cell.

III. SIMULATIONS OF EQUILIBRIUM WITH ION DIAMAGNETIC CURRENT

A. Initial state

Let us reproduce the profiles of plasma density, magnetic field strength and electric current which are realized in the equilibrium state with $\beta = 1$ predicted in Ref. 31. According to Kotelnikov, transition to the regime $T_e \to 0$ justifies the possibility of neglecting both the electric field and the electron drift current associated with it and allows to take into account only a diamagnetic current carried by massive ions ($m_i \gg m_e$).

We will compare theoretical predictions with the results of PIC simulations for the case when, in the region of zero magnetic field ($x < 0$), plasma ions have a Maxwellian velocity distribution, and the boundary between the plasma and the field is flat. The only component of the magnetic field is then expressed in terms of y-component of the vector potential $B = \partial A_y/\partial x$. Following Ref. 31, the ion distribution function in the transition layer $x > 0$ should have the form

$$f_i(x, \mathbf{v}) = \frac{n_0}{2\pi v_T^2} \exp\left(-\frac{v^2}{2v_T^2}\right)\mathcal{H}\left(\sin\theta - 1 + g(x)\frac{v_T}{v}\right), \quad (2)$$

where $\mathbf{v} = (v\cos\theta, v\sin\theta, 0)$ is the ion velocity vector, n_0 is the plasma density at $x < 0$, $g(x) = eA_y/(m_i c v_T)$ is the dimensionless potential of the magnetic field, and $v_T = \sqrt{T_i/m_i}$ is the ion thermal velocity. Solving the Maxwell equation with the current calculated from the distribution function (2), one can obtain the following implicit dependence of the vector potential g on the coordinate x:

$$x = \int_0^g du \left(\frac{4\sqrt{2}}{\pi}\int_0^{u^2/16} ds e^{-s}\mathcal{K}_{-1/4}(s)\right)^{-1/2}. \quad (3)$$

The coordinate x here is assumed to be measured in units of c/ω_{pi}, where $\omega_{pi} = \sqrt{4\pi e^2 n_0/m_i}$ is the plasma frequency of the ions, and $\mathcal{K}_{-1/4}(s)$ is the modified Bessel function. Knowing $g(x)$, we determine the profiles of the plasma density, electric current, and magnetic field as follows:

$$\frac{n}{n_0} = \frac{1}{2}e^{-g^2/8} + \frac{1}{\pi}\int_{g^2/8}^{\infty} ds e^{-s}\arcsin\left(1 - \frac{g}{\sqrt{2s}}\right), \quad (4)$$

$$-\frac{J_y}{en_0 v_T} = \frac{g}{2\sqrt{2\pi}}e^{-g^2/16}\mathcal{K}_{-1/4}(g^2/16), \quad (5)$$

$$\frac{B}{B_v} = g'/\sqrt{2}. \quad (6)$$

These profiles are graphically shown in Fig. 3. The presented profiles satisfy the pressure balance condition $\Pi_{xx} + B^2/(8\pi) = $ const, so the magnetic field can also be calculated using the following formula:

$$\frac{B(x)}{B_v} = \left(\frac{2\sqrt{2}}{\pi}\int_0^{g^2/16} ds e^{-s}\mathcal{K}_{-1/4}(s)\right)^{1/2}, \quad (7)$$

where $B_v = \sqrt{8\pi n_0 T_i}$ is the vacuum magnetic field. In units of $m_e c\omega_{pe}/e$, this field can be calculated as

$$B_v = \sqrt{\frac{2T_i}{m_e c^2}}. \quad (8)$$

B. Development of instability

Let us consider the equilibrium described above as the initial state of plasma and observe its further temporal evolution via PIC simulations. Figure 4 shows that, by the moment $\omega_{pe}t = 400$, the equilibrium distribution function in case 1 is perturbed by the wave with the y-polarized electric field while the same equilibrium in case 2 remains
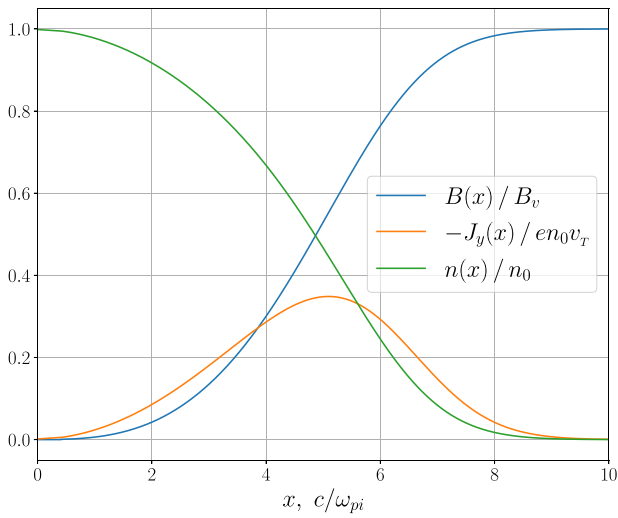
FIG. 3. Spatial profiles of plasma density, electric current, and magnetic field in equilibrium plasma with distribution function (2).

stable at this time. The field E_x observed at the plasma periphery in case 2 is due to a slight initial imbalance produced by finite-temperature electrons. The total energy of electric field demonstrates the exponential growth in case 1 and establishes at the constant level of thermal noise in case 2 [Fig. 4(h)]. The reason for this difference is the homogeneity of the system in z-direction in case 2, which prohibits the growth of periodic perturbations traveling along the ion drift. Further, we will study only the case 1 where the instability is allowed.

As seen from Fig. 4(c), at the initial stage of instability growth, there are perturbations with different spatial scales. Small-wavelength perturbations are excited in the electron cyclotron frequency band ($\omega \sim \Omega_e$). They appear earlier, propagate with the local drift velocity of ions and rapidly absorbed by electrons resulting in their heating. These high-frequency oscillations are completely damped by the time $\omega_{pe}t = 450$ and have almost no impact on the initial force balance. More intense perturbations with larger wavelengths ($\sim\rho_i$) grow at lower frequencies including the ion-cyclotron frequency harmonics Ω_i and the lower hybrid frequency Ω_{LH}.

Dynamics of this low-frequency instability up to the stage of non-linear saturation is presented in Fig. 5. One can see that the flute-like structure of perturbations at the linear stage of exponential growth is
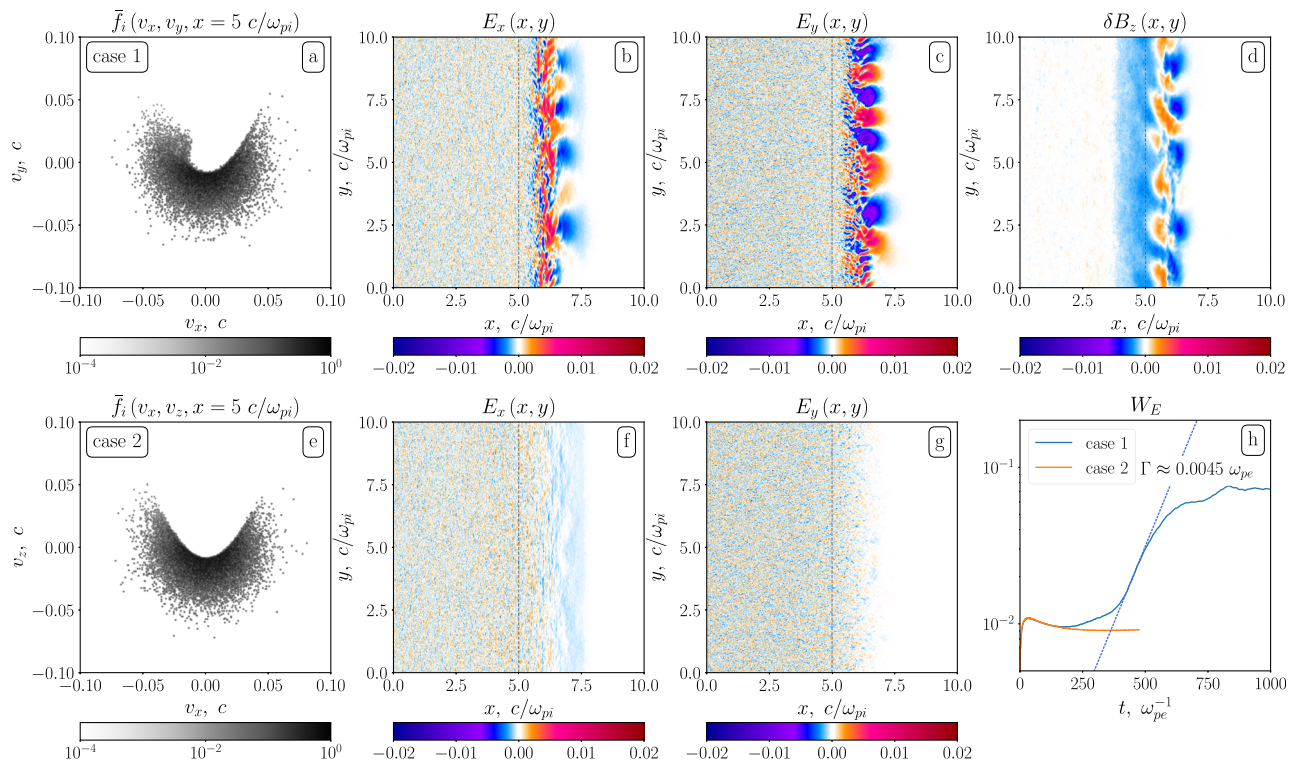

FIG. 4. Comparison between cases with different orientations of magnetic field in the moment of time $\omega_{pe}t = 400$ for the Kotelnikov equilibrium (upper row—case 1, bottom row—case 2): [(a) and (e)] y-averaged distribution functions of ions measured in the middle of the transition layer $x = 5\,c/\omega_{pi}$; [(b)–(d), (f), and (g)] (x, y)-maps of electromagnetic perturbations; (h) the total energy of electric field $W_E = \int |\mathbf{E}|^2 dxdy$ in case 1 (blue) and case 2 (orange) as a function of time (dashed blue line corresponds to exponential growth $e^{2\Gamma t}$ with $\Gamma = 0.0045\,\omega_{pe}$).
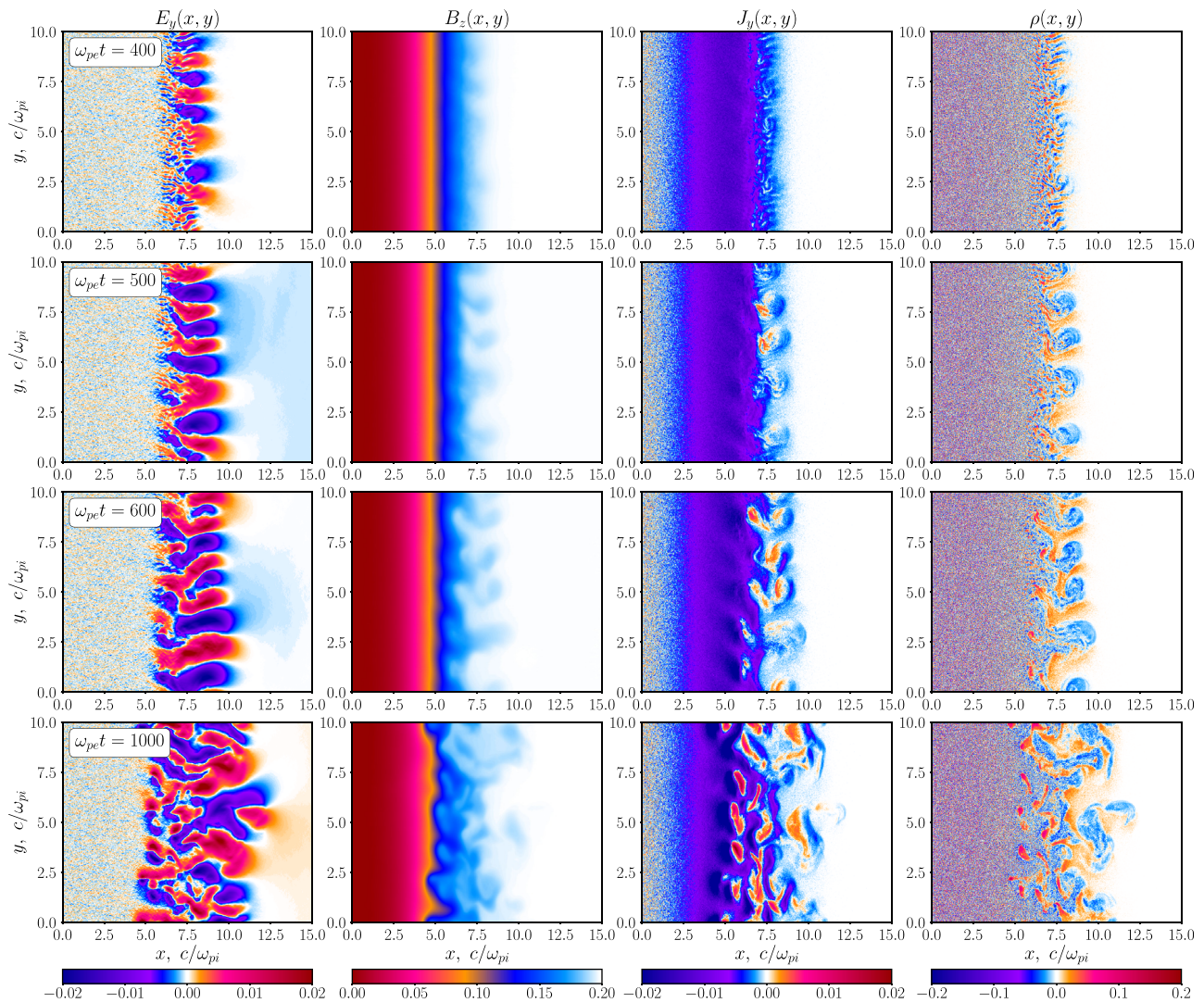
FIG. 5. Development of instability during the evolution of equilibrium (2)–(6) in PIC simulations: (first column) electric field $E_y(x, y)$, (second column) magnetic field $B_z(x, y)$, (third column) current density $J_y(x, y)$, and (fourth column) charge density $\rho(x, y) = n_i(x, y) - n_e(x, y)$.

transformed to the vortex structure at the saturation stage and becomes more turbulent at later times.

More detailed temporal evolution of electric and magnetic fields $E_y(y, t)$ and $\delta B_z(y, t)$ at different x-positions inside the current layer is shown in Fig. 6. It is seen that the typical time of instability growth is close to the period of one ion Larmor rotation ($2\pi/\Omega_i \approx 500\, \omega_{pe}^{-1}$). More precisely, the growth rate reaches the value $\Gamma = 0.0045\, \omega_{pe}$ [Fig. 4(h)] equal to a half of the local ion-cyclotron frequency ($\Gamma \approx \Omega_i(x)/2$) at the position of the most intense perturbations $x \approx 6\, c/\omega_{pi}$. The unstable discrete spectrum $k_y = 2\pi m/L_y$ is dominated by a few modes ($m = 3 - 6$) traveling in the direction of ion diamagnetic drift (negative y-direction). The maps of Fourier amplitudes $E_y(\omega, k_y)$ and $\delta B_z(\omega, k_y)$ show that the frequencies of growing modes lie near the several first harmonics of the local ion-cyclotron frequency $n\Omega_i(x)$ with $n = 1 - 4$. The unstable perturbations are

found to be electromagnetic ($|\delta B_z| \gg |E_y|$) in dense plasma regions ($\beta \sim 1$) and electrostatic ($|\delta B_z| \ll |E_y|$) at the periphery of the plasma ($\beta \ll 1$). To clarify if the most unstable modes belong to the drift branch, we draw the lines $k_y V_d(x)$ on the (ω, k_y)-plane with the local drift velocities $V_d(x) = J_y^i(x)/(en_i(x))$. Since the ion drift velocity reduces compared to the initial equilibrium value as the instability develops, resonance between the cyclotron harmonics and the drift branch is realized inside the finite angle sectors (between $k_y V_d^{\min}$ and $k_y V_d^{\max}$) rather than along the lines corresponding to the initial drift velocities $k_y V_d^{\max}$. Fourier (ω, k_y)-spectra presented in Fig. 6 confirm the drift nature of the instability observed.

As one can see from Fig. 6, the local lower hybrid frequency also lies in the range occupying by unstable waves. Nevertheless, we are inclined to call this instability ion-cyclotron, since the frequency of the most unstable modes remains constant when the selected x–position
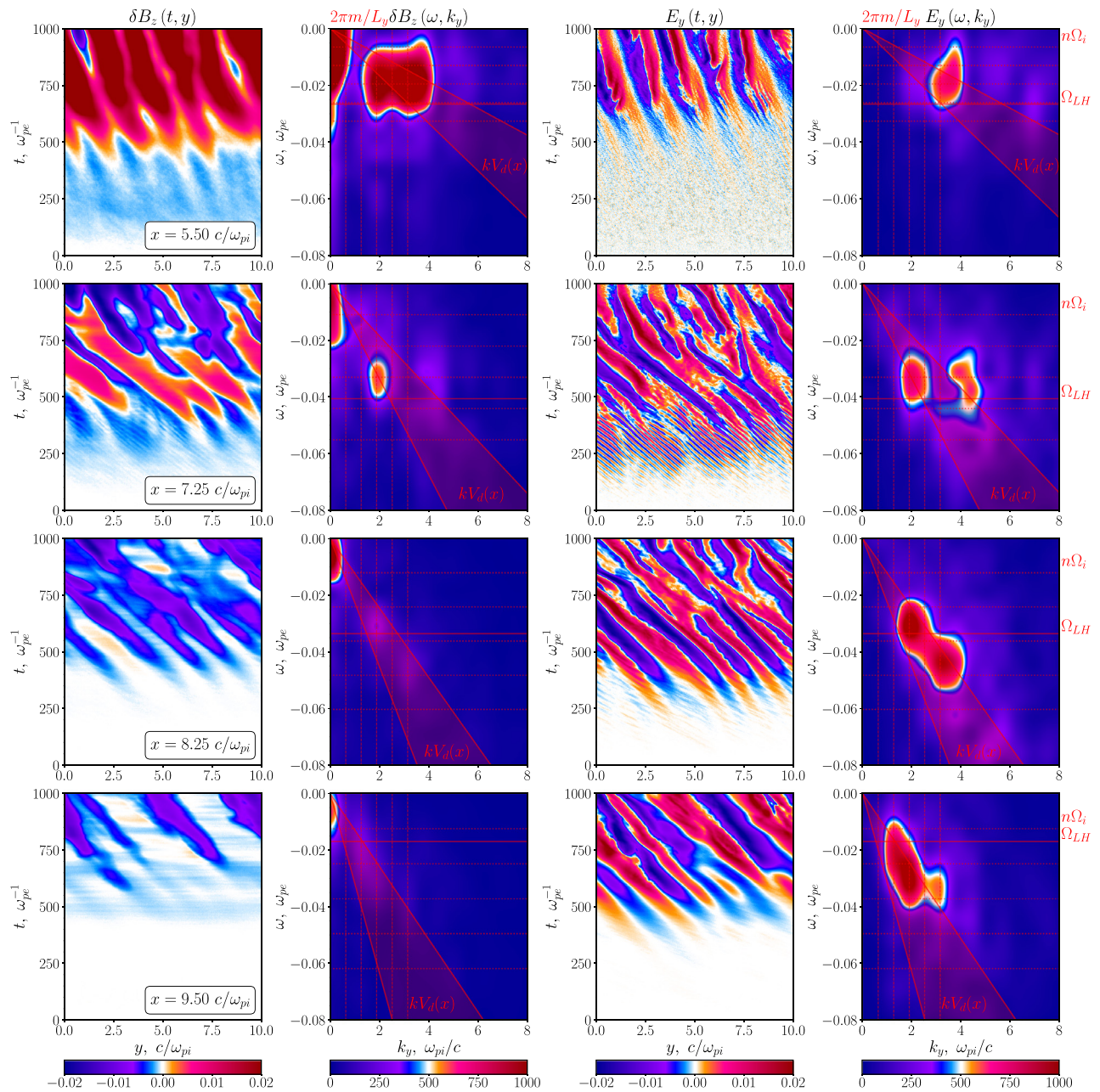
FIG. 6. Spatiotemporal evolution of magnetic $\delta B_z(t, y)$ (first column) and electric $E_y(t, y)$ (third column) perturbations along the selected x-positions in the Kotelnikov equilibrium and corresponding Fourier spectra $\delta B_z(\omega, k_y)$ (second column) and $E_y(\omega, k_y)$ (fourth column). Vertical red lines show positions of spatial discrete modes $k_y = 2\pi m/L_y$, and horizontal lines show positions of local cyclotron frequency harmonics $n\Omega_i(x)$ (dotted) and the lower hybrid frequency $\Omega_{LH}(x)$ (solid). Oblique lines indicate local drift frequencies calculated from the maximum $k_y V_d^{\max}$ and minimum $k_y V_d^{\min}$ ion drift velocities measured inside the time interval $\omega_{pe}t \in (0, 1000)$.

moves from $x = 7.25\,c/\omega_{pi}$ to $x = 9.5\,c/\omega_{pi}$. Indeed, the ion-cyclotron harmonics experience a little change in this part of the transition layer, while the lower hybrid frequency undergoes significant changes due to a strong decrease in density.

    Summarizing our study on the initial stage of instability development, we can conclude that the transition layer with ion diamagnetic current predicted by Kotelnikov[31] is unstable against perturbations at the ion-cyclotron frequency harmonics ($\omega \in (\Omega_i(x), 4\Omega_i(x))$). At the linear stage, unstable oscillations grow with the rate comparable to the real part of the frequency ($\Gamma \sim \Omega_i$) and propagate with the velocity of ion diamagnetic drift ($\omega/k \approx V_d$). This instability is very similar to the drift ion-cyclotron instability discussed by Mikhailovskii,[12] but a

detailed comparison with these theoretical predictions hardly makes sense, since the ion distribution in our transition layer is essentially non-Maxwellian and cannot be well approximated by the local Maxwellian function assumed in theory.

A similar instability of high-β plasma boundary, but with the unconventional direction of drift wave propagation (along the $\mathbf{E} \times \mathbf{B}$-drift of electrons rather than along the diamagnetic drift of ions), was observed earlier in simulations of plasma flow impingement on a growing magnetic field.[13] In the remaining part of this paper, we will show that the unstable waves can really propagate along the electron drift if the plasma is injected into the vacuum magnetic field and the current needed for equilibrium is produced by electrons from the very beginning. A similar situation is realized when the plasma flows into the growing magnetic field. In this case, electrons should also react faster than ions to appearance of electric field caused by charge separation and should produce the $\mathbf{E} \times \mathbf{B}$-drift current more rapidly than ions create a diamagnetic current.

C. Transition to equilibrium with electron current

Let us now investigate the influence of the observed instability on the equilibrium force balance. The unstable drift oscillations tend to diminish drift current that is initially carried by ions. Indeed, after mixing the plasma inside the current layer, the spectrum of unstable oscillations becomes rather wide and their phases chaotically changes on the typical spatial scale $\sim\rho_i$. Under these conditions, moving along its gyro-orbit, the ion must experience random forces from the electric field and pressure gradient that should result in the suppression of its directed drifts. Simulations show that during the development of instability in the transition layer, the ion current monotonically decreases, while an electric field E_x caused by charge separation gradually increases. Since the typical wavelength of ion-cyclotron perturbations is too large to affect the electron transport, the electrons begin to drift in the crossed fields E_x and B_z, thereby creating the current necessary for equilibrium. As a result, at the nonlinear stage of instability, we observe an almost complete replacement of the ion current with the initially smooth profile by an electron current concentrated in the individual filaments with a size of $\sim\rho_i$. Thus, the initial equilibrium state, in which the ion pressure force is compensated by the Ampère force,

$$-\frac{\partial \Pi_{xx}^i}{\partial x} + \frac{J_y^i B}{c} = 0 \qquad (9)$$

passes into a state where the ion current is minimized and the electric field transverse to the layer boundary is generated. The ion pressure force is then compensated by the electric force

$$-\frac{\partial \Pi_{xx}^i}{\partial x} + en_i E_x = 0, \qquad (10)$$

and the equilibrium of electrons in this electric field is provided by the Ampère force

$$-en_e E_x + \frac{J_y^e B}{c} = 0. \qquad (11)$$

Figure 7 presents some x-profiles of several quantities involved in equilibrium equations in the moment of time $\omega_{pe} t = 1700$. Local profiles at two different y-positions [averaged over the small vicinities of lines shaded in gray in Figs. 7(a)–7(c)] as well as profiles averaged over

the whole y-region are shown. Figures 7(d)–7(f) confirm that the ion current is strongly reduced compared to its initial value indicated by the dashed orange curve, and the current responsible for the magnetic field jump is almost completely produced by electrons. The electron drift current is indeed distributed over the separate filaments with a size of $\sim\rho_i$ which results in significant local deviations of magnetic field profiles from the equilibrium one [Figs. 7(g) and 7(h)]. Despite of these local deviations, the typical global size of the transition layer remains unchanged [Fig. 7(i)]. At both y-positions, the forces acting on ions do really satisfy the approximate equation (10) [see Figs. 7(j) and 7(k)], and the force balance for electrons is really well described by Eq. (11) [see Figs. 7(m) and 7(n)]. The presence of electron pressure gradient force with the comparable magnitude [Figs. 7(m) and 7(n)] but without visible influence on the stationary balance (11) is apparently a non-stationary effect which disappears after averaging over all y [Fig. 7(o)].

Note that in the previous works, where electrons also played a dominant role in creating the equilibrium current, the width of the transition layer was small ($\lambda \sim \rho_e$ in Ref. 30 and $\lambda \sim \sqrt{\rho_e \rho_i}$ in Ref. 2) and this did not allow the ions to perform a full Larmor rotation inside the layer. In the regime we considered in this work, the transition layer remains wide ($\lambda \approx 10\,\rho_i$), and the ion drift motion is suppressed by the developed ion-cyclotron instability.

IV. SIMULATIONS OF PLASMA INJECTION IN VACUUM MAGNETIC FIELD

Let us find out whether the high-β equilibrium remains stable if it is created gradually during a continuous increase in plasma pressure in a given space region.

A. Development of instability

PIC simulations with continuous plasma injection show that the equilibrium (10) and (11) characterized by the strong electric field and purely electron current establishes from the very beginning in this problem. Electrons react to appearance of electrostatic potential faster than ions perform the Larmor rotation. Therefore, the $\mathbf{E} \times \mathbf{B}$–drift current of electrons dominates the ion diamagnetic current from the early stage of injection when the plasma pressure has not yet grown to large values ($\beta \ll 1$). Layers of electron current initially localized at the plasma boundaries with the width $\lambda < \rho_i$ (upper row in Fig. 8) turn out to be unstable against the same ion-cyclotron perturbations that have been observed during evolution of the Kotelnikov's equilibrium (Sec. III B). Figure 8 shows that the initially thin current sheet is first mixed on the scale of the ion Larmor radius, and then its size increases to $(5 - 6)\rho_i$.

The spectral analysis of growing perturbations presented in Fig. 9 demonstrates that the observed instability is very similar to the instability developing in the ion diamagnetic current layer of Kotelnikov. Indeed, the frequency ω of unstable drift waves lies near the first ion-cyclotron harmonics $n\Omega_i$ with $n = 1 - 3$, and the typical wavenumber k_y along the drift direction has the same value $\sim\omega_{pi}/c$. The only difference is that the unstable oscillations propagate now along the direction of electron $\mathbf{E} \times \mathbf{B}$–drift (positive y-direction) rather than in the direction of ion diamagnetic drift (negative y-direction). This "unconventional" direction of drift waves propagation was also observed in earlier PIC simulations[13] when a directed plasma flux was injected toward the growing magnetic field. This fact seems to be
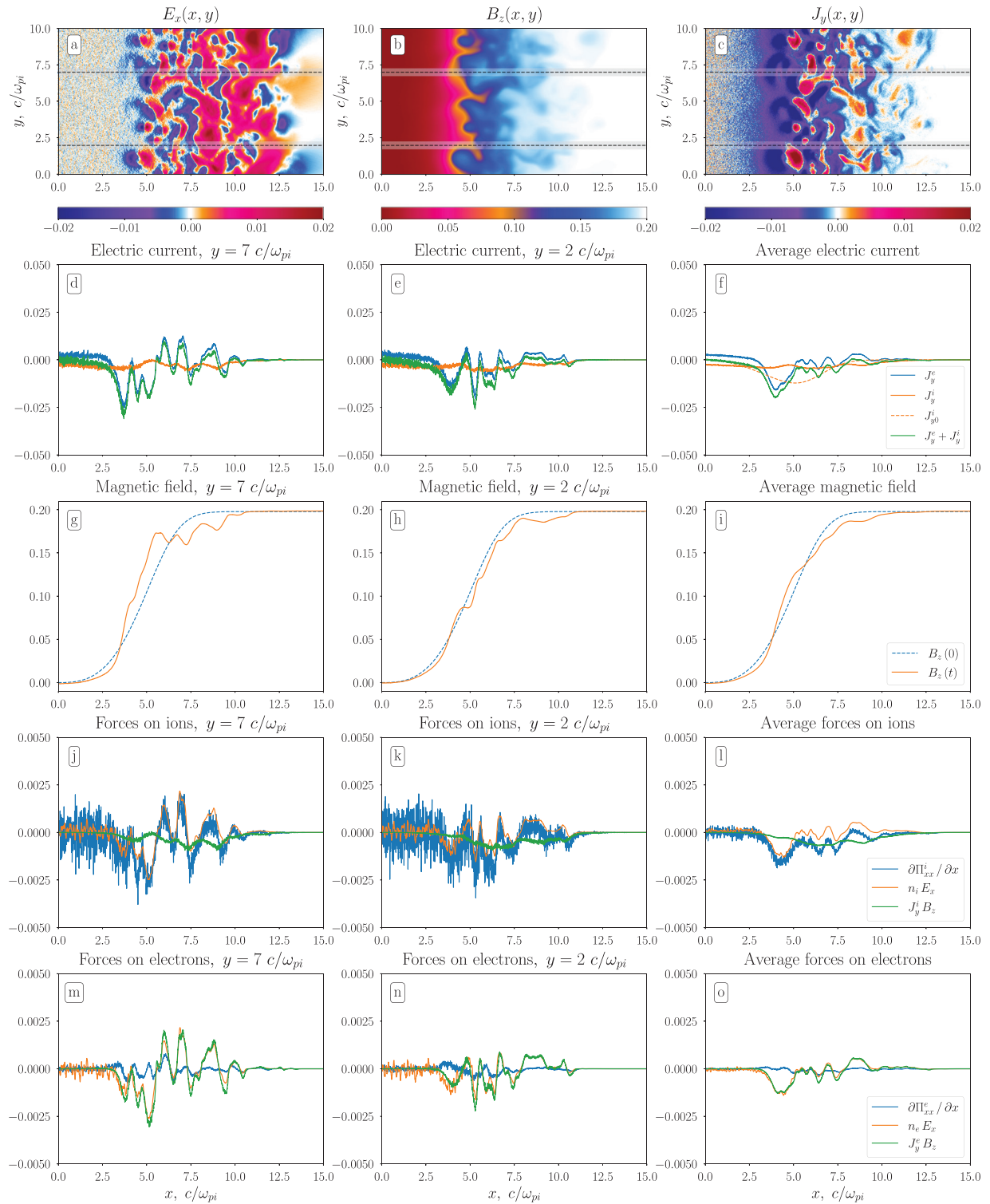
FIG. 7. New equilibrium state in the PIC model in the moment $\omega_{pe}t = 1700$: (a)–(c) maps of electric field $E_x(x, y)$, magnetic field $B_z(x, y)$, and current $J_y(x, y)$ (lines show y-positions where we measure local x-profiles); (d)–(f) local and averaged over y profiles of currents $J_y^{i,e}(x)$ produced by different particle species; (g)–(i) local and averaged over y profiles of magnetic field $B_z(x)$; (j)–(l) balance of forces (local and averaged over y) acting on ions; and (m)–(o) the same balance for electrons.
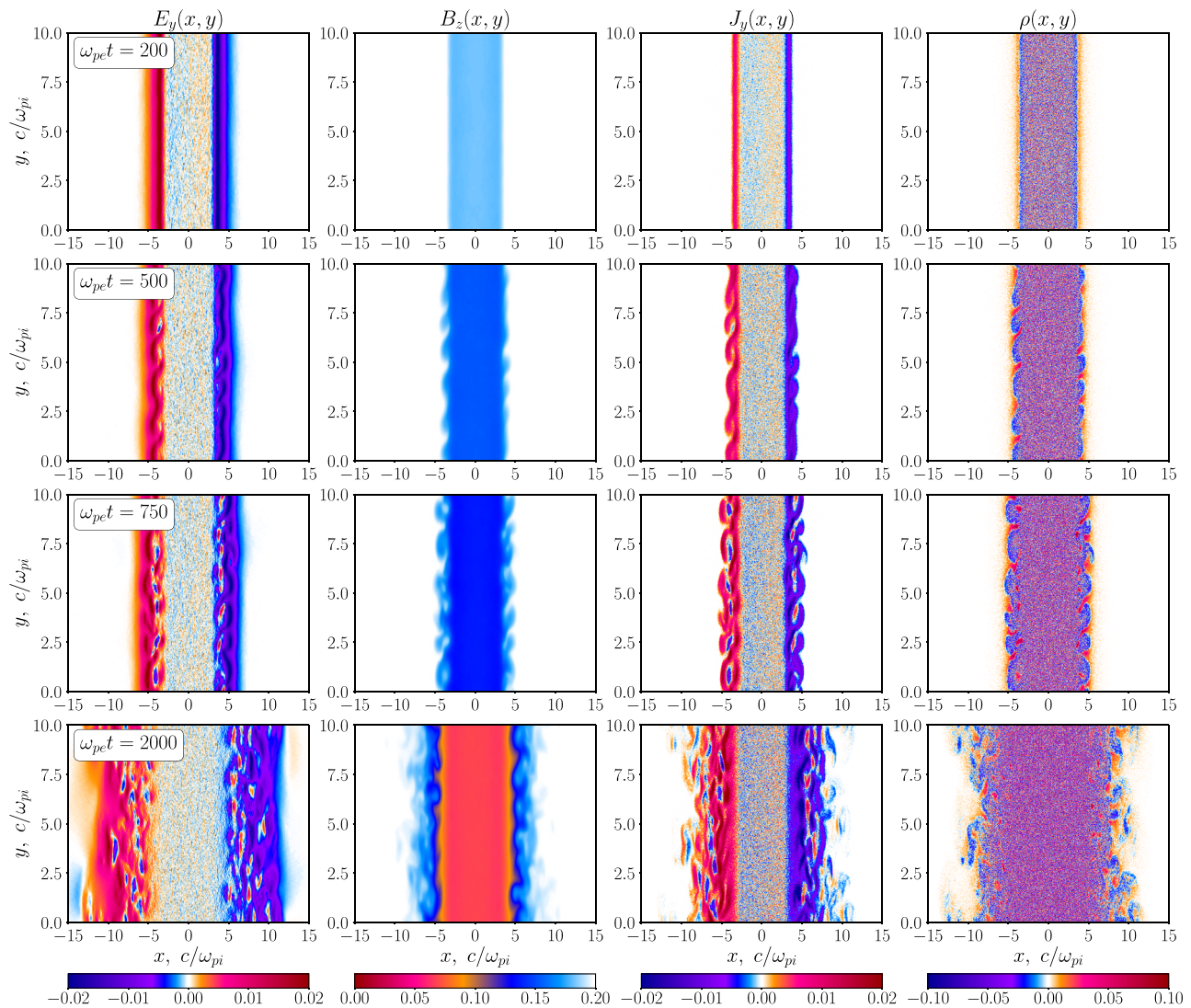
FIG. 8. Development of instability at boundaries of the injection region: maps of electric field $E_y(x, y)$ (first column), maps of magnetic field $B_z(x, y)$ (second column), maps of electric current $J_y(x, y)$ (third column), and maps of charge density $\rho(x, y) = n_i(x, y) - n_e(x, y)$ (fourth column).

unconventional if only we imagine that the ion pressure is balanced by the ion diamagnetic current (indeed, the unstable Kotelnikov's equilibrium, dominated initially by the ion current, excites waves along the ion drift in agreement with theoretical predictions[12]) but it becomes natural when the equilibrium current is completely produced by the electron drift (the ion pressure is balanced by the jump of electrostatic potential from the very beginning in this case, and all ion drifts are greatly suppressed by collective interaction with unstable waves).

Since the plasma density at the selected x-position, where we observe the instability, varies from zero to $\simeq 0.5$ during the instability growth, the local lower hybrid frequency Ω_{LH} changes in a rather wideband (shaded in blue in Fig. 9) which covers the entire region of the unstable spectrum. Thus, it is impossible to separate contributions from drift instabilities at Ω_{LH} and $n\Omega_i$.

B. Force balance

At the initial stage of injection, when the plasma pressure β inside the injection region has not yet grown to unity, we observe the same force balance to which the Kotelnikov equilibrium comes when the instability saturates. Indeed, the current is almost completely created by electrons [Fig. 10(c)], the ion pressure gradient force is compensated by the electric force [Fig. 10(f)], and the electric force acting on electrons is balanced by their Ampère force [Fig. 10(e)].

At the same time, as seen from Fig. 10(d), the relative plasma pressure $\beta(t) = 2\Pi_{xx}/B_v^2$ does not grow according to the linear law with which the energy $W_{inj}(t) = n_0(T_i + T_e)t/\tau$ is injected into the system. On the one hand, a slower growth is demonstrated by the plasma density due to spreading of the ions beyond the injection region to a distance of their Larmor radius. However, we will not be
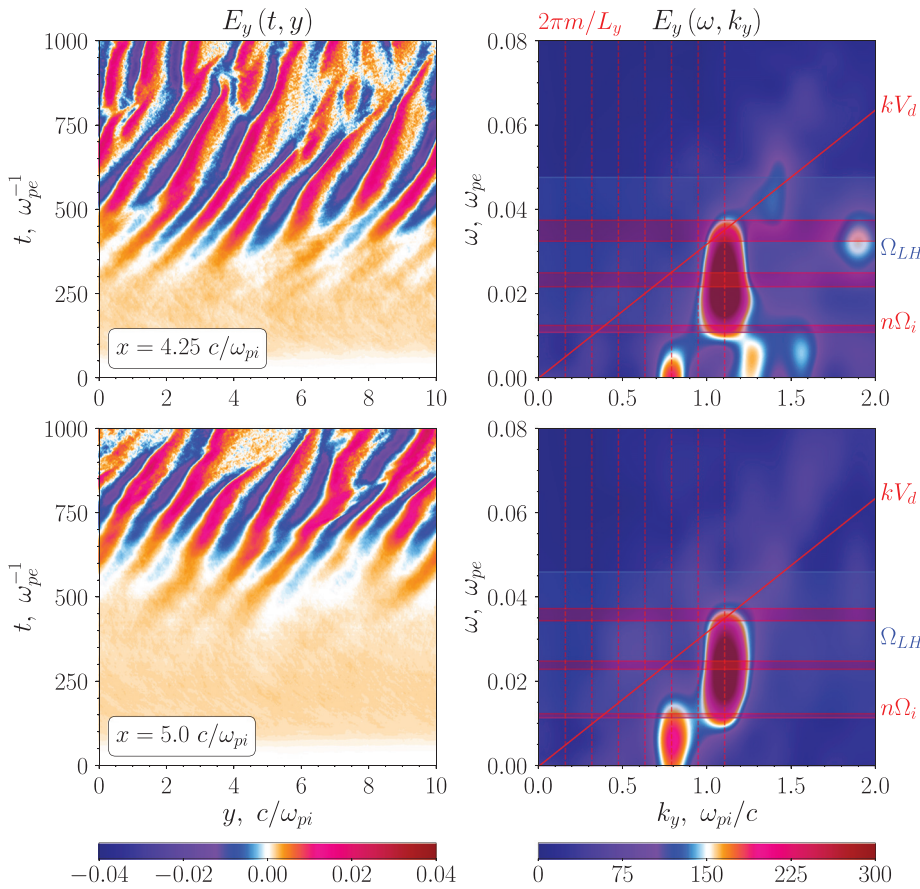
FIG. 9. Spatiotemporal evolution of electric field perturbations $E_y(t, y)$ at different x-positions near the boundary of the injection region (first column) and corresponding Fourier spectra $E_y(\omega, k_y)$ (second column). Vertical red lines indicate positions of discrete modes $k_y = 2\pi m/L_y$. Straps shaded in red show local ion-cyclotron harmonics $n\Omega_i$ varying during the selected time window, the blue strap—the lower hybrid frequency. The oblique line corresponds to the drift frequency $k_y V_d$ calculated from the average electron drift velocity.

able to explain the slowdown in the growth of β observed in PIC simulations in the center of the injection region $x = 0$ [Fig. 10(d)], even if we calculate the plasma pressure taking into account the real dynamics of its local density, $P_T = n_i(t, 0)T_i + n_e(t, 0)T_e$ [dashed blue curve in Fig. 10(d)]. A direct calculation of the momentum flux carried by plasma particles from their distribution functions measured in the PIC model,

$$\Pi_{xx}(t, 0) = \sum_{s=e,i} \int m_s v_x^2 f_s(t, 0, \mathbf{v}) d\mathbf{v}, \qquad (12)$$

shows that this value [orange curve in Fig. 10(d)] is indeed noticeably lower than the pressure P_T obtained under the assumption of constant temperatures T_i and T_e. At the same time, Π_{xx} coincides with the change in the magnetic field pressure observed in PIC simulations [green curve in Fig. 10(d)], which can be calculated as

$$\Delta P_B = \int_{-\infty}^{x} J_y(x')B_z(x')dx' = \frac{B_v^2 - B^2}{2}. \qquad (13)$$

The difference between Π_{xx} and P_T at this stage can be explained by the adiabatic decrease in the energy of previously injected particles together with a decrease in the local magnetic field in which they perform their Larmor rotation. Indeed, at the stage when the magnetic field has not yet decreased too much compared to the vacuum field,

the Larmor radius of the ions turns out to be smaller than the half-width of the injection region, and the change in the magnetic field can be considered slow compared to the ion gyroperiod. Under these conditions, the conservation of the adiabatic invariant ($\mu \propto T/B = const$) suggests that by the time t the effective temperature of the ions injected at the time t' decreases to the value $T_i(t) = T_i B(t)/B(t')$.

With further deepening of the magnetic well, we pass to the regime when the Larmor radius $\rho_i = (c/\omega_{pi})B_v/B$ begins to exceed the half-width of the injection region $l = 3.125\, c/\omega_{pi}$, and the plasma pressure inside this region becomes close to the limit $\beta = 1$. In this case, the magnetic field exclusion slows down drastically, and the injected power is spent more on the expansion of the magnetic well than on its deepening [in Fig. 11(b) the pressure profile stopped growing and only expands]. If the half-width of the magnetic well in PIC simulations is determined from the position of the half-maximum of Π_{xx}-profile [Fig. 11(b)], then the typical well size w grows almost linearly in time as shown in Fig. 11(d) (orange curve). If we also take into account a decrease in ion temperature inside the injection region, the typical Larmor radius of ions ($\rho_i(t) = (c/\omega_{pi})B_v/B(t)\sqrt{T_i(t)/T_i(0)}$), shown in Fig. 11(d) as a green curve, remains smaller than the well size w during the whole process we consider. It means that most of particles from the central part of the plasma $x = 0$ never reach the transition layer with large ∇B, and their magnetic moment is conserved.
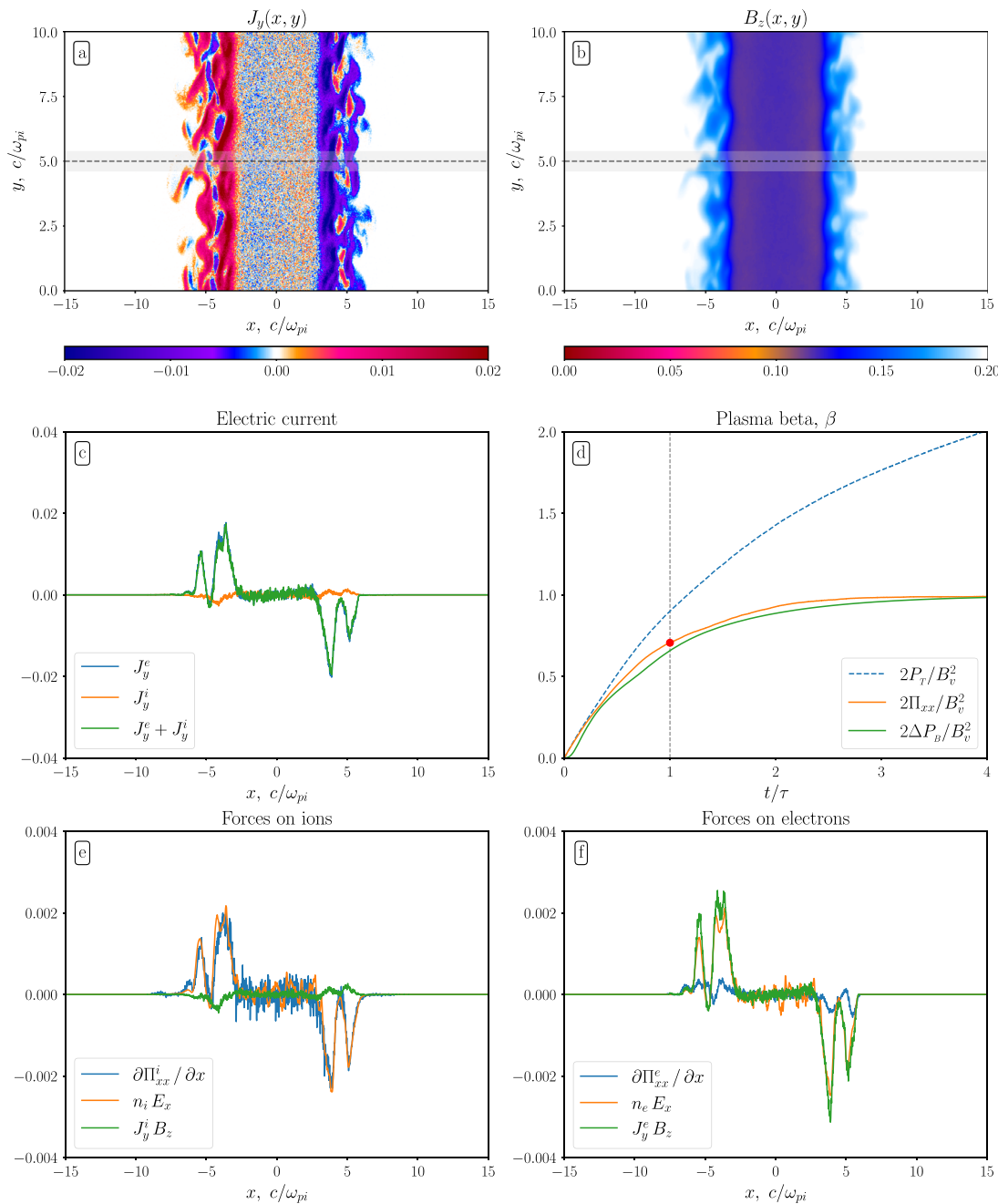
FIG. 10. Results of PIC simulations at the early stage of plasma injection $t = \tau$: (a) map of electric current $J_y(x, y)$ (dashed line shows the position where the local force balance is studied, shaded band is the interval of y-averaging); (b) map of magnetic field $B_z(x, y)$; (c) local x-profiles of current produced by different particle species; (d) y-averaged plasma β in the center of injection region ($x = 0$) as a function of time calculated from P_T, Π_{xx}, and ΔP_B; (e) local balance of forces acting on ions; and (f) local balance of forces acting on electrons.

The turbulent layer ($|x| \geq w$), in which the equilibrium (10) and (11) is still realized [Figs. 11(e) and 11(f)], also shifts along with the well edge, but inside the well ($l < x < w$), we observe the formation of density and pressure gradients free of turbulent mixing, which allows ions to have a drift current there. As can be seen from Fig. 11(c), such a current does actually appear in the central part of the well ($|x| < w$); however, this current is directed not toward the ion drift under the action of its pressure gradient, but in the direction of the $\mathbf{E} \times \mathbf{B}$-drift. The oppositely flowing current required to balance the ion pressure is still created by the electrons [Fig. 11(c)]. Inside the injection region ($|x| < l$), plasma pressure is
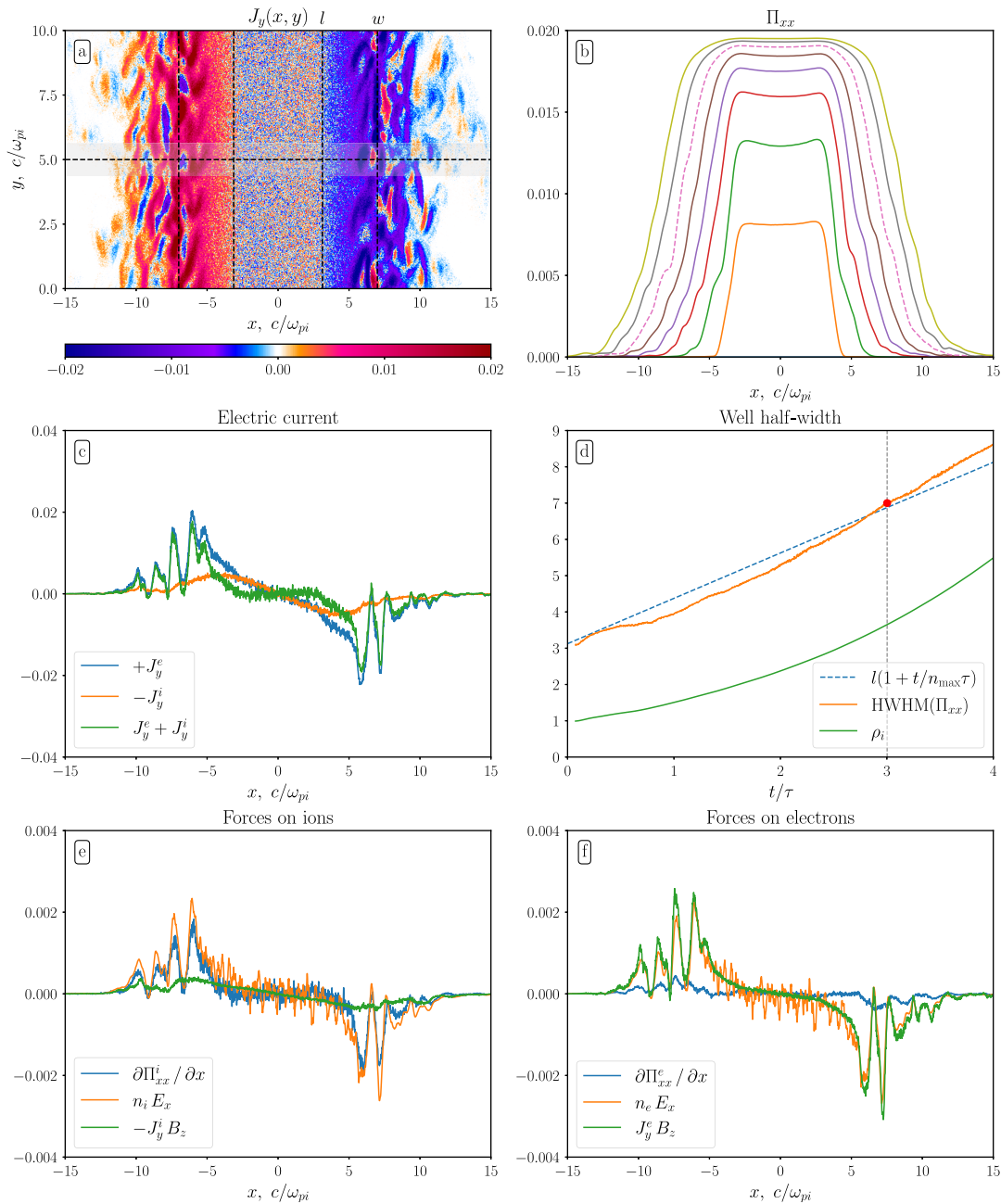
10 November 2023 04:47:15

FIG. 11. Results of PIC simulations at the stage of β saturation ($t = 3\tau$): (a) map of electric current $J_y(x, y)$ (horizontal dashed line shows the position where the local force balance is studied, and vertical lines show boundaries of the injection region l and the half-width of the magnetic well w); (b) evolution of plasma (Π_{xx}) or magnetic (ΔP_B) pressure profiles in time with the interval $\tau/2$; (c) local x-profile of currents $J_y^{e,i}$ produced separately by ions and electrons; (d) history of magnetic well size $w(t)$ observed in PIC simulations and predicted in theory as well as growth of the ion Larmor radius $\rho_i(t)$ at $x = 0$; (e) local x-profiles of force acting on ions; and (f) local x-profiles of force acting on electrons.

uniform, and the growing ion current is completely created by the $\mathbf{E} \times \mathbf{B}$–drift of ions ($en_iE_x + J_y^iB_z/c = 0$). The appearance of such a current in a homogeneous injection region is explained as follows. Due to the conservation of the generalized momentum $p_y = m_iv_y + e/cA_y$, ions can reach a turbulent layer with a sufficiently large magnetic field only at sufficiently large negative values of m_iv_y. After collective interaction with

unstable oscillations, these ions are trapped in the transition layer, carrying this momentum away from the central region of the plasma. Averaging over the particles remaining in the Maxwellian distribution of the central plasma gives a nonzero positive flux.

Thus, our PIC simulations show that the transition layer with the dominant electron current is also unstable against ion-cyclotron

oscillations in the problem when plasma pressure gradually increases to the limit $\beta = 1$. After the development of this instability, the typical width of this layer grows up to the same value $10\,\rho_i$ as in the kinetic equilibrium predicted by Kotelnikov. We also show that the closer the plasma pressure approaches the magnetic field pressure, the wider the magnetic well becomes and the slower the magnetic field is excluded from it. In particular, this means that, in the z-homogeneous system, even an arbitrarily long plasma injection into a selected region of space will not result in reaching a zero magnetic field. To confirm this tendency, we will try to describe temporal evolution of the magnetic well theoretically.

V. DYNAMICS OF MAGNETIC FIELD AT THE WELL BOTTOM

The rate of magnetic field exclusion from the injection region observed in our PIC simulations can be explained within the framework of the following simple model. Let us first find the law of the plasma density growth inside the injection region. Over time dt, the increase in plasma density equals to

$$dn(t) = \frac{dt}{\tau} f(a) \sqrt{\frac{B(t)}{B(t')}}. \tag{14}$$

Here, we take into account two effects that slow down the linear growth of plasma density during continuous injection of particles: (i) smearing particles in space described by the factor $f(a)$, and (ii) conservation of magnetic moment of each particle resulting in appearance of the square root multiplier (t' is the moment of particle injection).

If plasma particles were uniformly injected into infinite space with a stationary magnetic field, the plasma density would have to reach the value $n = 1$ at time $t = \tau$. In our case, however, the injection region is spatially limited; therefore, the density at the center of the injection region should decrease when particles scatter from this region along their cyclotron orbits to distances of the Larmor radius. It is obvious that the magnitude of this decrease should depend on the ratio of the Larmor radius ρ to the half-width of the injection region l ($a = l/\rho$). For the uniform magnetic field and Maxwellian distribution of injected particles, the function of their smearing can be calculated exactly as follows:

$$f(a) = 2\int_0^\infty w e^{-w^2} n(a, w) dw, \tag{15}$$

where

$$n(a, w) = \begin{cases} 1, & 0 < w < \frac{a}{2}, \\ \frac{1}{2} + \frac{\theta}{\pi} + \frac{1}{\pi^2}\int_\theta^{\pi-\theta} A d\varphi, & \frac{a}{2} < w < a, \\ \frac{1}{2} - \frac{\theta}{\pi} + \frac{1}{\pi^2}\int_{-\theta}^{\pi+\theta} A d\varphi, & a < w < \infty, \end{cases} \tag{16}$$

$$A = \arcsin\left(\frac{a}{w} - \sin\varphi\right), \quad \theta = \arcsin\left|\frac{a}{w} - 1\right|.$$

However, to simplify analytical formulas, we will use the following approximation for the exact function $f(a)$,

$$\tilde{f}(a) = \frac{1}{1 + \alpha/a}, \tag{17}$$

which has a simple interpretation. Indeed, after gyro-averaging, particles occupy a region with the larger size $l + \alpha\rho$, where α is a numerical coefficient. Due to the conservation of particles number, plasma spreading should be accompanied by a decrease in its density by a factor $l/(l + \alpha\rho)$ that coincides with $\tilde{f}(a)$. From the comparison of asymptotic behavior of exact and approximate functions $f(a)$ and $\tilde{f}(a)$ in the limit of large Larmor radii ($a \ll 1$), one can conclude that the best value for the numerical coefficient is $\alpha = 0.55$ (Fig. 12), but better agreement with PIC simulations is achieved at another value $\alpha = \sqrt{\pi}/4$.

Another effect that slows down the linear growth of plasma density inside the injection region is associated with the adiabatic increase in Larmor radius of previously injected particles in a gradually deepening magnetic well. Indeed, in the 1D problem, the plasma density decreases with the growth of ρ as $n \propto 1/\rho$ because of the conservation of particles number. If the slowly varying system also admits the conservation of the magnetic moment, the change in the Larmor radius of a particle in a falling magnetic field is contributed not only by a reduction in the cyclotron frequency but also by a change in its velocity. In this case, the density of particles dn injected in the moment t' should decrease to the value $dn\sqrt{B(t)/B(t')}$ by the moment of observation t. Therefore, the plasma density accumulated in the injection region by the time t is determined by the following integral:

$$n(t) = \frac{\sqrt{b(t)}}{\tau}\int_0^t \frac{dt'}{\sqrt{b(t')}} f(a'), \tag{18}$$

where $a' = lb(t')$, the plasma density is measured in units of n_0, spatial sizes—in c/ω_{pi}, and $b(t) = B(t)/B_v$ is the dimensionless magnetic
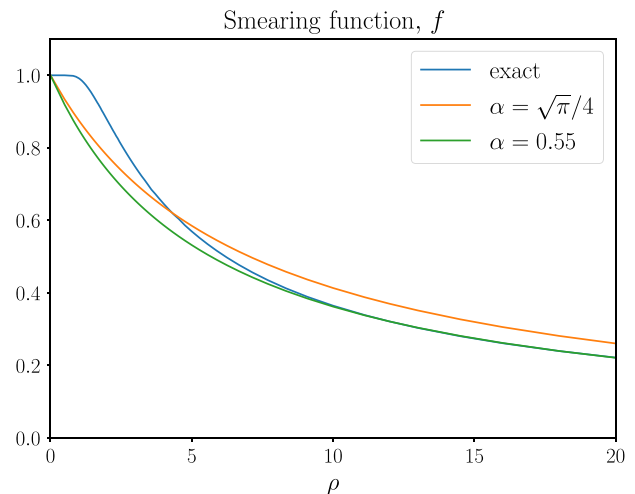

FIG. 12. Comparison of the exact smearing function $f(l/\rho)$ for the fixed size of injection region $l = 3.125\,c/\omega_{pi}$ with the approximate function $\tilde{f}$ at $\alpha = \sqrt{\pi}/4$ and $\alpha = 0.55$.

field in the center of the injection region. To obtain the law of plasma pressure growth, it is necessary to take into account that the effective temperature of the injected particles decreases with the decrease in magnetic field because of the magnetic moment conservation:

$$\Pi_{xx} = \frac{(T_i + T_e)b^{3/2}(t)}{\tau} \int_0^t \frac{dt'}{b^{3/2}(t')} f(a'), \quad (19)$$

where T_i and T_e are the dimensionless ion and electron temperatures in units of $m_e c^2$. On the other hand, at each moment of time, the equilibrium equation must be satisfied

$$\Pi_{xx} = \Delta P_B = \frac{B_v^2}{2}(1 - b^2(t)). \quad (20)$$

Since $T_i = B_v^2/2$, the final equation for the time evolution of the magnetic field at the well bottom $b(t)$ takes the form

$$\frac{1}{\tau_0} \int_0^t \frac{dt'}{b^{3/2}(t')} f(a') = \frac{1-b^2}{b^{3/2}}, \quad (21)$$

where $\tau_0 = \tau/(1 + T_e/T_i)$. The solution to this equation can be presented in an implicit form

$$\frac{t}{\tau_0} = \frac{1}{2} \int_{b(t)}^1 \frac{(x + 3/x)}{f(lx)} dx. \quad (22)$$

If we use approximation $\tilde{f}(a)$ instead of exact function $f(a)$, the above integral can be calculated analytically as follows:

$$\frac{t}{\tau_0} = \frac{1-b^2}{4} - \ln b^{3/2} + \frac{\alpha}{2l}(1-b)\left(1 + \frac{3}{b}\right). \quad (23)$$

The plasma density and its relative pressure at any time can be expressed in terms of the magnetic field as follows:

$$n(t) = \frac{\tau_0}{\tau}\left[\frac{\sqrt{b}}{3}(1 - b^{3/2}) + 3(1 - \sqrt{b})\right], \quad (24)$$

$$\beta(t) = 1 - b^2. \quad (25)$$

It is seen from Fig. 13 that the theory based on the exact $f(a)$ appears to be more accurate at the early stage of injection ($t < \tau$) while the

later history of $b(t)$, $n_i(t)$, and $\beta(t)$ is better described by the approximate function $\tilde{f}(a)$ with $\alpha = \sqrt{\pi}/4$.

In the limit $t \to \infty$, the magnetic well ceases to fit into the computational domain chosen for our PIC simulations; however, the theory predicts the following asymptotic behavior of the magnetic field strength:

$$b(t) \to \frac{3\alpha\tau_0}{2lt}. \quad (26)$$

If we assume that the temperature is constant and the magnetic moment is not conserved, this asymptotic is reduced by a factor 3/2.

At late stages, the plasma density asymptotically approaches a constant value $n_{\max} = 3/(1 + T_e/T_i)$, and the continuous plasma injection with the rate $n_{\max}\dot{w}(t) = l/\tau$ is entirely spent on the linear increase in the typical size of the magnetic well $w(t)$:

$$w(t) \to l\left(1 + \frac{t}{n_{\max}\tau}\right). \quad (27)$$

Figure 11(d) shows that this linear law is close to the corresponding dependence measured in PIC simulations even when the density has not yet saturated. Thus, in a non-dissipative system that is uniform along the vacuum magnetic field, this field is not completely excluded from the injection region and the magnetic well expands infinitely. In a more realistic formulation of the problem, when the system is limited in all three directions and Coulomb collisions are taken into account, the restriction on reaching a zero magnetic field inside the injection region is, of course, removed and the magnetic well size stops to grow at a finite value. Note that the magnetic field was observed to be completely expelled from the laser-produced plasma in the cusp experiments.[43,44]

VI. SUMMARY

In this paper, we study the stability of a plasma equilibrium with $\beta = 1$,[31] in which the diamagnetic current is carried by relatively hot ions ($T_i \gg T_e$). PIC simulations of such an equilibrium state show that, regardless of the electron temperature, the transition layer in this plasma turns out to be unstable against perturbations at ion-cyclotron frequency harmonics $\omega = (1-4)\Omega_i$ propagating with the phase velocity close to the drift velocity of ions. The observed instability is similar in nature to the drift ion-cyclotron instability of Mikhailovskii and Timofeev[12] with the only difference that it develops in a plasma with the strongly non-Maxwellian ion distribution providing large drift velocities $V_d = (1-7)v_T$. It is also found that the equilibrium of
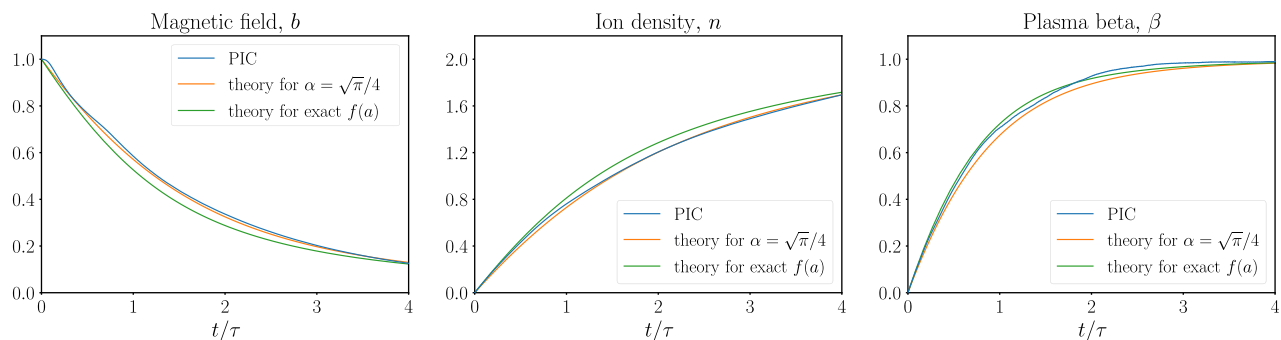

FIG. 13. Comparison of theoretical predictions for the magnetic field $b(t)$, ion density $n_i(t)$, and plasma pressure $\beta(t)$ at the center of the injection region with the results of PIC simulation. Theories based on both the exact $f(a)$ and approximate $\tilde{f}(a)$ (with $\alpha = \sqrt{\pi}/4$) smearing functions are presented.

interest remains stable if the plasma in our 2D simulations is assumed homogeneous in the drift direction of particles. This raises a question about the possibility of forming a current layer with an electron Larmor radius scale that has been observed in axially symmetric PIC simulations[30] incapable of resolving perturbations of azimuthal drifts. Unfortunately, to answer the question whether the favorable curvature of magnetic field lines in a cusp may stabilize this instability, it is necessary to perform 3D simulations.

It is also interesting that the development of the drift ion-cyclotron instability accompanied by plasma mixing on the local Larmor radius scale suppresses the ion current and favors a transition to the new state where the ion pressure is balanced by the electric potential, and the current necessary for the equilibrium is created by the electron $\mathbf{E} \times \mathbf{B}$-drift. In contrast to previous works, in which the dominance of electrons in the creation of currents was associated with a small thickness of the transition layer, in our case the layer remains wide, and the main reason for the suppression of ion drifts is the development of instability at the ion-cyclotron frequency harmonics.

The conclusion about instability of a transition layer, which is formed in configurations with the high plasma pressure, seems to be very important for the confinement of fast ions in the regime of diamagnetic bubble inflation in mirror traps. However, it is unclear whether the Kotelnikov equilibrium studied here can be formed or whether it remains stable in a more realistic way of creating plasma, when the increase in plasma pressure to the limiting value $\beta = 1$ occurs gradually due to, for example, the continuous high-energy neutral injection. To clarify this point, we simulate a more realistic problem of continuous plasma injection into a selected region of space with an initially uniform magnetic field. It is found that the boundary transition layer with a current created from the beginning by the $\mathbf{E} \times \mathbf{B}$–drift of electrons is unstable against the same drift perturbations at the ion-cyclotron frequency harmonics that was observed in the Kotelnikov equilibrium. The only difference is the propagation direction of the unstable drift waves which now travel along the electron drift. At the initial stage of injection ($1 - \beta \sim 1$), the ion pressure is balanced by a jump of electrostatic potential and ions do not create current, since their drifts are greatly suppressed by unstable oscillations. At the later stage ($1 - \beta \ll 1$), the deepening of the magnetic well slows down and the well becomes much wider than the injection region. In the central part of this expanding well there is no turbulence, which allows ions to produce an electric current. This current does really appear, but it flows not under the pressure gradient, but in the opposite direction of the $\mathbf{E} \times \mathbf{B}$–drift. In this case, electrons not only compensate this positive current of ions, but also produce a negative current required for balancing the ion pressure.

Thus, in the absence of losses, the continuous plasma injection results in the formation of the expanding magnetic well with the unstable transition layer of typical size $\lambda \simeq 10\rho_i$. Using the simple theoretical model, we explained the rate at which the magnetic field is excluded from the injection region and showed how this process slows down when the magnetic moment is conserved.

ACKNOWLEDGMENTS

AUTHOR DECLARATIONS
Conflict of Interest

The authors have no conflicts to disclose.

Author Contributions

Vladislav Kurshakov: Software (lead); Validation (lead); Visualization (lead); Writing – original draft (equal). **Igor Timofeev:** Conceptualization (lead); Formal analysis (lead); Supervision (equal); Writing – original draft (equal).

DATA AVAILABILITY

The data that support the findings of this study are available from the corresponding author upon reasonable request.

REFERENCES

[1]S. Chapman and V. C. A. Ferraro, "A new theory of magnetic storms," J. Geophys. Res. **36**, 171, https://doi.org/10.1029/TE036i003p00171 (1931).

[2]V. C. A. Ferraro, "On the theory of the first phase of a geomagnetic storm: A new illustrative on an idealized (plane not cylindrical) model field distribution," J. Geophys. Res. **57**, 15, https://doi.org/10.1029/JZ057i001p00015 (1952).

[3]D. M. Willis, "Structure of the magnetopause," Rev. Geophys. **9**, 953, https://doi.org/10.1029/RG009i004p00953 (1971).

[4]D. M. Willis, "The microstructure of the magnetopause," Geophys. J. R. Astron. Soc. **41**, 355 (1975).

[5]M. N. Rosenbluth, "Dynamics of a pinched gas," in *Magnetohydrodynamics*, edited by R. K. M. Landshoff (Stanford University Press, Stanford, CA, 1957), p. 57.

[6]R. L. Morse, "Adiabatic time development of plasma sheaths," Phys. Fluids **8**, 308 (1965).

[7]R. L. Morse, "Adiabatic time development of linear theta-pinch plasma profile," Phys. Fluids **10**, 1560 (1967).

[8]M. G. Haines, "Plasma containment in cusp-shaped magnetic fields," Nucl. Fusion **17**, 811 (1977).

[9]V. P. Pastukhov, "Anomalous electron transport in the transition layer of an electrostatically plugged magnetic mirror," Sov. J. Plasma Phys. **6**, 549–554 (1980).

[10]H. Grad, "Boundary layer between a plasma and a magnetic field," Phys. Fluids **4**, 1366 (1961).

[11]G. Schmidt and D. Finkelstein, "Magnetically confined plasma with a Maxwellian core," Phys. Rev. **126**, 1611 (1962).

[12]A. B. Mikhailovskii and A. V. Timofeev, "Theory of cyclotron instability in a non-uniform plasma," Sov. Phys. JETP **17**(3), 626 (1963).

[13]J. Berchem and H. Okuda, "A two-dimensional particle simulation of the magnetopause current layer," J. Geophys. Res. **95**(6), 8133, https://doi.org/10.1029/JA095iA06p08133 (1990).

[14]D. W. Hewett, C. W. Nielson, and D. Winske, "Vlasov confinement equilibria in one dimension," Phys. Fluids **19**, 443 (1976).

[15]N. A. Krall and P. C. Liewer, "Low-frequency instabilities in magnetic pulses," Phys. Rev. A **4**, 2094 (1971).

[16]R. C. Davidson and N. A. Krall, "Anomalous transport in high-temperature plasmas with applications to solenoidal fusion systems," Nucl. Fusion **17**(6), 1313 (1977).

[17]R. C. Davidson, N. T. Gladd, C. S. Wu, and J. D. Huba, "Effects of finite plasma beta on the lower-hybrid-drift instability," Phys. Fluids **20**, 301 (1977).

[18]D. Winske and P. C. Liewer, "Particle simulation studies of the lower hybrid drift instability," Phys. Fluids **21**, 1017 (1978).

[19]E. A. Kuznetsov, T. Passot, V. P. Ruban, and P. L. Sulem, "Variational approach for static mirror structures," Phys. Plasmas **22**, 042114 (2015).

[20]H. Gota, M. W. Binderbauer, T. Tajima, S. Putvinski, M. Tuszewski, B. H. Deng, S. A. Dettrick, D. K. Gupta, S. Korepanov, R. M. Magee *et al.*, "Formation of hot, stable, long-lived field-reversed configuration plasmas on the C-2W device," Nucl. Fusion **59**, 112009 (2019).

[21] S. A. Dettrick, D. C. Barnes, F. Ceccherini, L. Galeotti, S. A. Galkin, S. Gupta, K. Hubbard, O. Koshkarov, C. K. Lau, Y. Mok *et al.*, "Simulation of equilibrium and transport in advanced FRCS," Nucl. Fusion **61**, 106038 (2021).

[22] Y. Peng, Y. Yang, Y. Jia, B. Rao, M. Zhang, Z. Wang, H. Wang, and Y. Pan, "Simulation on formation process of field-reversed configuration," Nucl. Fusion **62**, 066037 (2022).

[23] T. J. Dolan, "Magnetic electrostatic plasma confinement," Plasma Phys. Controlled Fusion **36**, 1539 (1994).

[24] J. Park, N. A. Krall, P. E. Sieck, D. T. Offermann, M. Skillicorn, A. Sanchez, K. Davis, E. Alderson, and G. Lapenta, "High-energy electron confinement in a magnetic cusp configuration," Phys. Rev. X **5**, 021024 (2015).

[25] A. D. Beklemishev, "Diamagnetic 'bubble' equilibria in linear traps," Phys. Plasmas **23**, 082506 (2016).

[26] M. S. Khristo and A. D. Beklemishev, "High-pressure limit of equilibrium in axisymmetric open traps," Plasma Fusion Res. **14**, 2403007 (2019).

[27] M. S. Khristo and A. D. Beklemishev, "Two-dimensional MHD equilibria of diamagnetic bubble in gas-dynamic trap," Plasma Phys. Controlled Fusion **64**, 095019 (2022).

[28] J. Egedal, D. Endrizzi, C. B. Forest, and T. K. Fowler, "Fusion by beam ions in a low collisionality, high mirror ratio magnetic mirror," Nucl. Fusion **62**, 126053 (2022).

[29] B. A. Wetherton, A. Le, J. Egedal, C. Forest, W. Daughton, A. Stanier, and S. Boldyrev, "A drift kinetic model for the expander region of a magnetic mirror," Phys. Plasmas **28**, 042510 (2021).

[30] J. Park, G. Lapenta, D. Gonzalez-Herrero, and N. A. Krall, "Discovery of an electron gyroradius scale current layer: Its relevance to magnetic fusion energy, Earth's magnetosphere, and sunspots," Front. Astron. Space Sci. **6**, 74 (2019).

[31] I. Kotelnikov, "On the structure of the boundary layer in a Beklemishev diamagnetic bubble," Plasma Phys. Controlled Fusion **62**, 075002 (2020).

[32] Y. A. Omelchenko and H. Karimabadi, "Spontaneous generation of a sheared plasma rotation in a field-reversed θ-pinch discharge," Phys. Rev. Lett. **109**, 065004 (2012).

[33] D. I. Skovorodin, "Gas dynamic multiple mirror trap GDMT," Plasma Phys. Rep. **49**(9), 1039–1086 (2023).

[34] P. A. Bagryansky, A. D. Beklemishev, and V. V. Postupaev, "Encouraging results and new ideas for fusion in linear traps," J. Fusion Energy **38**(1), 162 (2019).

[35] P. A. Bagryansky, T. D. Akhmetov, I. S. Chernoshtanov, P. P. Deichuli, A. A. Ivanov, A. A. Lizunov, V. V. Maximov, V. V. Mishagin, S. V. Murakhtin, E. I. Pinzhenin *et al.*, "Status of the experiment on magnetic field reversal at BINP," AIP Conf. Proc. **1771**, 030015 (2016).

[36] Y. Tsidulko and I. S. Chernoshtanov, "Particle-in-cell simulation of field reversal in mirror trap with neutral beam injection," AIP Conf. Proc. **1771**, 040005 (2016).

[37] W. C. Turner, J. F. Clauser, F. H. Coensgen, D. L. Correll, W. F. Cummins, R. P. Freis, R. K. Goodman, A. L. Hunt, T. B. Kaiser, G. M. Melin, W. E. Nexsen, T. C. Simmonen, and B. W. Stallard, "Field-reversal experiments in a neutral-beam-injected mirror machine," Nucl. Fusion **19**(8), 1011 (1979).

[38] I. S. Chernoshtanov, "Collisionless particle dynamics in diamagnetic trap," Plasma Phys. Rep. **48**(2), 79 (2022).

[39] J. P. Boris, "Relativistic plasma simulation-optimization of a hybrid code," in *Proceedings of 4th Conference on Numerical Simulations of Plasmas, Washington, DC, 2–3 November* (Naval Research Laboratory, 1970), pp. 3–67.

[40] K. Yee, "Numerical solution of initial boundary value problems involving Maxwell's equations in isotropic media," IEEE Trans. Antennas Propag. **14**(3), 302–307 (1966).

[41] T. Esirkepov, "Exact charge conservation scheme for particle-in-cell simulation with an arbitrary form-factor," Comput. Phys. Commun. **135**, 144–153 (2001).

[42] V. V. Annenkov, E. A. Berendeev, I. V. Timofeev, and E. P. Volchok, "High-power terahertz emission from a plasma penetrated by counterstreaming different-size electron beams," Phys. Plasmas **25**, 113110 (2018).

[43] A. Kitsunezaki, M. Tanimoto, and T. Sekiguchi, "Cusp confinement of high-beta plasmas produced by a laser pulse from a freely-falling deuterium ice pellet," Phys. Fluids **17**, 1895 (1974).

[44] R. E. Pechacek, J. R. Greig, M. Raleigh, D. W. Koopman, and A. W. DeSilva, "Measurement of the plasma width in a ring cusp," Phys. Rev. Lett. **45**(4), 256 (1980).